Journal of Solid State Chemistry 226 (2015) 126–132

Contents lists available at ScienceDirect

Journal of Solid State Chemistry

journal homepage: www.elsevier.com/locate/jssc

Crystal structure and properties of tetragonal $EuAg_4In_8$ grown by metal flux technique

Udumula Subbarao, Sumanta Sarkar, Sebastian C. Peter*

New Chemistry Unit, Jawaharlal Nehru Centre for Advanced Scientific Research, Jakkur, Bangalore 560064, India

ARTICLE INFO

Article history:
Received 24 December 2014
Received in revised form
8 February 2015
Accepted 15 February 2015
Available online 25 February 2015

Keywords:
Intermetallics
Crystal structure
Crystal growth
Magnetism
Resistivity

ABSTRACT

The compound $EuAg_4In_8$ has been obtained as single crystals in high yield from reactions run in liquid indium. X-ray diffraction on single crystals suggests that $EuAg_4In_8$ crystallizes in the $CeMn_4Al_8$ structure type, tetragonal space group $I4/mmm$ with lattice constants $a=b=9.7937(2)$ Å and $c=5.7492(2)$ Å. Crystal structure of $EuAg_4In_8$ is composed of pseudo Frank–Kasper cages occupied by one europium atom in each ring, which are shared through the corner along the *ab* plane resulting in a three dimensional network. The magnetic susceptibility of $EuAg_4In_8$ was measured in the temperature range 2–300 K, which obeyed Curie–Weiss law above 50 K. Magnetic moment value calculated from the fitting indicates the presence of divalent europium, which was confirmed by X-ray absorption near edge spectroscopy. Electrical resistivity measurements suggest that $EuAg_4In_8$ is metallic in nature with a probable Fermi liquid behavior at low temperature.

1. Introduction

Among the rare earths intermetallics, the Eu-containing compounds deserve particular scientific interest as they can exhibit two energetically similar electronic configurations; the nonmagnetic Eu^{3+} ($4f^6$) and the magnetic Eu^{2+} ($4f^7$). Eu based compounds exhibit various important properties such as intermediate valency, heavy fermion behavior, Kondo behavior, unusual magnetism [1–6] and superconductivity at low temperature [7,8]. These properties are generally believed to arise from the strong hybridization (interaction) between the localized *4f* electrons and the delocalized *s*, *p*, and *d* conduction electrons [9,10].

Structural aspects of many intermetallic compounds interestingly depend on the way the compound is synthesized, which in most of the cases may indirectly affect the physical properties of the material as structure and property are intriguingly related to each other. Metal flux method has not only been proved to be a tremendous tool to grow single crystals of already known polycrystalline compounds for studying detailed physical properties but also been an effective way to explore completely new phases [11–21]. A classic example in this case is EuInGe. Mao et al. [22] reported that this compound crystallizes in orthorhombic *Pnma* space group when the compound was synthesized in high frequency induction heating; we in our previous work, however, found out that this compound crystallizes in monoclinic $P2_1/c$ space group [23]. Similarly, $YbCuGa_3$ was previously reported to have crystallized in tetragonal $I4/mmm$ structure when synthesized by the arc melting method [24]; however it was later found to have monoclinic structure (space group, $C2/m$) when synthesized using Ga as an active flux [25].

Here we report another compound $EuAg_4In_8$ which was previously reported by Sysa et al. [26] in the hexagonal crystal system with space group $P6/mmm$, which is unusual in the RET_4X_8 (*RE*=Rare earths, *T*=Transition metals, *X*=p-block elements) family. Based on the literature and our previous reports on $YbCu_4Ga_8$ [27], $YbCu_6In_6$ [28] and $SmCu_6In_6$ [29], we know that the family of these compounds crystallizes mostly in the tetragonal crystal system with space group $I4/mmm$. Sysa et al. have synthesized the compound by arc-melting, which is not an efficient technique for the synthesis of Eu based compounds due to high vapor pressure of Eu. They have reported the divalent state of Eu in $EuAg_4In_8$ with the help of X-ray absorption L_{III}-spectra analysis. In continuation to our studies in the RET_4X_8 family and related compounds in this series, we found that $EuAg_4In_8$ exists in tetragonal phase as well. The other motivation of this work is that the compounds having general formula RET_4X_8 (*RE*=La–Nd, Sm–Lu and U; *T*=Cr, Mn, Fe, Cu and Ag; *X*=Al, Ga and In) are generally well known for their interesting physical properties like high temperature antiferromagnetic ordering (T_N) in $GdFe_4Al_8$ [30] ($T_N=155$ K) along with two low temperature transitions at $T_1=21$ K and $T_2=27$ K, high temperature magnetic ordering (163.5 K) in $TbFe_4Al_8$ [31], anisotropic magnetic properties of single crystals of UFe_4Al_8 [32] and the antiferromagnetic–paramagnetic transitions at $T_N=6.50$ and 6.75 K in $GdCr_xAl_{12-x}$ ($x=3.5$ and 4.0) [33].

* Corresponding author. Tel.: +91 80 22082998; fax: +91 80 22082627.
E-mail address: sebastiancp@jncasr.ac.in (S.C. Peter).

http://dx.doi.org/10.1016/j.jssc.2015.02.013
0022-4596/

As per Inorganic Crystal Structure Database (ICSD) [34] and Pearson's Crystal Data (PCD) [35], $EuAg_4In_8$ is the only compound so far reported in the Eu–Ag–In system [26]. In addition, among the large number of RET_4X_8 compounds, only a few Eu based compounds were reported so far. The examples are $EuCu_4Al_8$ [36,37], $EuFe_4Al_8$ [38] and $EuMn_4Al_8$ [37]. All these compounds crystallize in the tetragonal $ThMn_{12}$ structure type (space group $I4/mmm$). Though there is a slight variation in composition, $EuFe_6Al_6$ [39,40] is another compound reported in the same structure type.

We also focused our research to develop the intermetallic chemistry of Eu based compounds [17,23,41–44], which in fact cause a few interesting properties. The single crystals of $EuAg_4In_8$ were grown using In as the active metal flux. The use of indium flux has been proved to be an excellent tool to produce many novel ternary and quaternary intermetallic phases [45–49]. A few new polyindides with an impressive set of diverse structures and compositions have been synthesized using In as solvent [45,46]. The crystal structure of $EuAg_4In_8$ was studied using single crystal X-ray diffraction data. Magnetic susceptibility and electrical resistivity studies were performed on the single crystals obtained by the metal flux method.

2. Experimental section

2.1. Reagents

The following reagents were used as purchased without further purification: Eu (in the form of metal pieces cut from metal chunk, 99.99% Alfa Aesar), Ag (powder, 99.99% Alfa Aesar) and In (pieces, 99.999%, Alfa Aesar).

2.2. Synthesis

2.2.1. Metal flux synthesis of $EuAg_4In_8$

Single crystals of $EuAg_4In_8$ were obtained by reacting europium metal (0.3 g), silver (0.28 g) and indium (2 g) in an alumina crucible. The crucible placed in a 13 mm fused silica tube was flame sealed under a vacuum of 10^{-3} Torr, to prevent oxidation during heating. The reactants were then heated to 1000 °C over 10 h, maintained at that temperature for 5 h to allow proper homogenization, then cooled to 850 °C in 2 h and kept at this temperature for 48 h. Finally, the sample was allowed to slowly cool down to 30 °C over 48 h. The reaction product was isolated from the excess indium flux by heating at 400 °C and subsequently centrifuging through a coarse frit. Any unreacted flux was removed by immersion and sonication in glacial acetic acid for 24 h. The final crystalline product was rinsed with water and dried with acetone. Small (0.5 mm) rod-shaped single crystals of $EuAg_4In_8$ were selected for the elemental analysis, structural characterization and property studies. Our attempts to synthesize the compound in bulk polycrystalline form using high frequency induction heating also resulted in the formation of $EuAg_4In_8$ as major product along with unreacted indium and $AgIn_2$ impurity phases (XRD pattern of the sample synthesized by induction furnace is shown in the Supporting information, Fig. S1).

2.3. Elemental analysis

Semi-quantitative microanalyses were performed on the single crystals obtained from the flux techniques using a Leica 220i scaning electron microscope (SEM) equipped with Bruker 129 eV energy dispersive X-ray analyzer (EDS). Data were acquired with an accelerating voltage of 20 kV and 90 s accumulation time. SEM image of a typical single crystal of $EuAg_4In_8$ is shown in Fig. 1. The EDS analyses were performed on visibly clean surfaces of the single crystals obtained from the flux method. The atomic composition obtained is 8(1):30(2):62(3) for Eu:Ag:In indicating that the atomic composition was close to 1:4:8, which is in good agreement with the composition obtained from the single crystal X-ray data refinement.

2.4. Powder X-ray diffraction

Phase identity and purity of the $EuAg_4In_8$ sample obtained from the metal flux method and high frequency induction heating were determined by powder XRD experiments that were carried out with a Bruker D8 Discover diffractometer using Cu-$K\alpha$ radiation ($\lambda = 1.5406$ Å). The experimental powder pattern of $EuAg_4In_8$ obtained from the metal flux method was found to be in good agreement with the pattern calculated from the single-crystal X-ray structure refinement of the tetragonal structure (Fig. 2). The high frequency induction heating produced a mixture of hexagonal and tetragonal phases (Fig. S1).

2.5. Single-crystal X-ray diffraction

X-ray diffraction data were collected on a selected single crystal of $EuAg_4In_8$ at room temperature using a Bruker Smart Apex 2-CCD diffractometer equipped with a normal focus, 2.4 kW sealed tube X-ray source with graphite monochromatic Mo-$K\alpha$ radiation ($\lambda = 0.71073$ Å) operating at 50 kV and 30 mA, with ω scan mode. A crystal of suitable size ($0.05 \times 0.05 \times 0.1$ mm^3) was cut from a rod shaped crystal and mounted on a thin glass (~0.1 mm) fiber with commercially available super glue. A full sphere of 120 frames was acquired up to 75.68° in 2θ. The individual frames were measured with steps of 0.5° and an exposure time of 60 s per frame. The program SAINT [50] was used

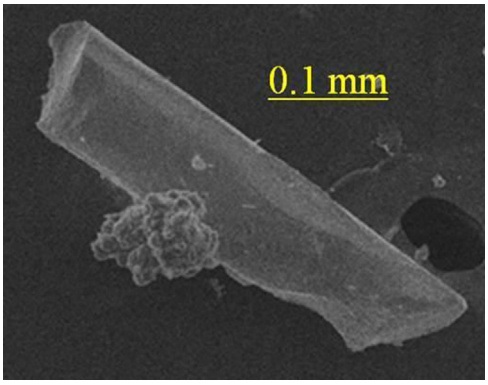

Fig. 1. SEM image of typical $EuAg_4In_8$ single crystal grown from In flux.

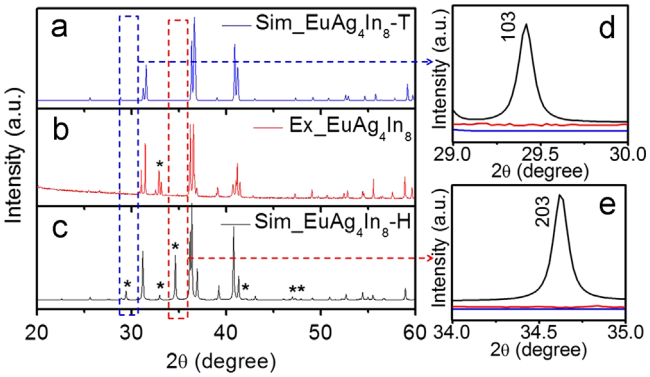

Fig. 2. PXRD comparison of simulated tetragonal and hexagonal systems with experimental $EuAg_4In_8$ (a) star mark corresponds to unreacted indium peak, (b) star peak corresponds to hexagonal crystal system and (d and e) correspond to two extra peaks (103 and 203 planes) are highlighted from hexagonal system. The peaks marked with * correspond to $AgIn_2$ phase.

for integration of diffraction profiles and absorption correction was made with SADABS program [51]. The systematic absences led to the centrosymmetric space group *I*4/*mmm*. However, the Platon program with WinGx system, ver. 1.80.05 [52] was used to check the additional symmetry, which confirms the final structure refinement. The structure was solved by SHELXS 97 [53] and refined by a full matrix least-squares method using SHELXL with anisotropic atomic displacement parameters for all atoms. Packing diagrams were generated with Diamond [54]. As a check for the correct composition, the occupancy parameters were refined in a separate series of least-squares cycles. All bond lengths are within the acceptable ranges compared to their theoretical values.

Since the structure was previously reported in the hexagonal system, our next intention was to collect the single crystal XRD data on available temperature range in our instrument. We have carried out the temperature dependent single crystal XRD studies using Bruker Photon 100 CMOS detector in shutter less mode equipped with a micro-focus, 5 kW sealed tube X-ray source with graphite monochromatic Mo-*K*α radiation (λ=0.71073 Å) operating at 50 kV and 1 mA, with ω scan mode at various temperatures 100 K, 200 K, 350 K and 450 K.

2.6. Structure refinement

The crystal structure of $EuAg_4In_8$ was refined using Shelxl-97 (full-matrix least-squares on F^2) [53] with anisotropic atomic displacement parameters for all atoms. As a check for the correct composition, the occupancy parameters were refined in a separate series of least-squares cycles. The first step of refinement showed that $EuAg_4In_8$ crystallizes in a body centered tetragonal lattice (*I*4/*mmm*) within the $CeMn_4Al_8$ structure type with lattice constants $a=b=9.7937(2)$ Å and $c=5.7492(2)$ Å. This refinement resulted in four crystallographic positions in the $EuAg_4In_8$ structure where one europium atom occupies 2*a* site, one silver atom occupies 8*f* site and two indium atoms occupy 8*i* and 8*j* sites. During the isotropic refinement of $EuAg_4In_8$, unacceptable highest difference peak and deepest hole (>12 and -11 e Å^3) were observed. The refinement residual value (R1) also was found to be slightly high (8%). Since the scattering power of Ag and In atoms to X-ray is close due to only two electron difference, we also attempted to refine the structure with Ag and In mixing; however, we did not improve the refinement parameters. To overcome all these problems observed in the refinement $EuAg_4In_8$, we have recollected the data with long exposure time (60 s) and more number of frames (120). This revised data collection overcame the problems associated with the initial data collection (10 s and within 30 frames).

The details of data collection and structure refinement are listed in Table 1. The standard atomic positions and isotropic atomic displacement parameters of this compound are given in Table 2. The anisotropic displacement parameters and important bond lengths are listed in Tables 3 and 4, respectively. Further information on the structure refinements is available : by quoting the Registry No. CCDC 1002249.

2.7. Magnetic measurements

Magnetic measurements of $EuAg_4In_8$ were carried out on a Quantum Design MPMS-SQUID magnetometer. Measurements were performed on single crystals, which were ground and screened by single crystal and powder XRD to verify phase identity and purity. Temperature dependent data were collected for field cooled mode (FC) between 2 and 300 K in an applied field (*H*) of 1000 Oe. Magnetization data were also collected for $EuAg_4In_8$ at 2 K and 300 K with field sweeping from -60 kOe to 60 kOe.

Table 1
Crystal data and structure refinement for $EuAg_4In_8$ at 296(2) K.

Empirical formula	$EuAg_4In_8$
Formula weight	1502
Wavelength	0.71073 Å
Crystal system	Tetragonal
Space group	*I*4/*mmm*
Unit cell dimensions	$a=b=9.7937(2)$ Å $c=5.7492(2)$ Å
Volume	551.44(3) Å^3
Z	2
Density (calculated)	9.04528 g/cm^3
Absorption coefficient	28.826 mm^{-1}
F(000)	1285.9
Crystal size	$0.05\times0.05\times0.10$ mm^3
θ range for data collection	2.94–45.35°
Index ranges	$-19\le h\le 19$ $-15\le k\le 17$ $-8\le l\le 11$
Reflections collected	3286
Independent reflections	686 [$R_{int}=0.0485$]
Completeness to $\theta=45.35°$	100%
Refinement method	Full-matrix least-squares on F^2
Data/restraints/parameters	686/0/16
Goodness-of-fit	1.181
Final *R* indices [$>2\sigma(I)$]	$R_{obs}=0.036$, $wR_{obs}=0.086$
Extinction coefficient	0.012793
Largest diff. peak and hole	2.728 and -4.887 e Å^{-3}

$R=\Sigma||F_o|-|F_c||/\Sigma|F_o|$, $wR=\{\Sigma[w(|F_o|^2-|F_c|^2)^2]/\Sigma[w(|F_o|^4)]\}^{1/2}$ and calc $w=1/[\sigma^2(Fo^2)+(0.0359P)^2+6.1794P]$ where $P=(Fo^2+2Fc^2)/3$.

Table 2
Atomic coordinates ($\times10^4$) and equivalent isotropic displacement parameters (Å$^2\times10^3$) for $EuAg_4In_8$ at 296(2) K with estimated standard deviations in parentheses.

Label	Wyckoff site	*x*	*y*	*z*	Occupancy	U^*_{eq}
Eu	2*a*	0	0	0	1	8 (1)
Ag	8*f*	2500	2500	2500	1	12 (1)
In1	8*i*	3471 (5)	0	0	1	12 (1)
In2	8*j*	2880 (9)	5000	0	1	20 (1)

Table 3
Anisotropic displacement parameters (Å$^2\times10^3$) for $EuAg_4In_8$ at 296(2) K with estimated standard deviations in parentheses.

Label	U_{11}	U_{22}	U_{33}	U_{12}	U_{13}	U_{23}
Eu	8 (1)	8 (1)	9 (1)	0	0	0
Ag	14 (2)	14 (2)	8 (1)	1 (1)	3 (1)	3 (1)
In1	11 (2)	10 (2)	15 (2)	0	0	0
In2	42 (2)	7 (1)	11 (2)	0	0	0

The anisotropic displacement factor exponent takes the form: $-2\pi^2[h^2a^{*2}U_{11}+\ldots+2hka^*b^*U_{12}]$.

Table 4
Selected bond lengths [Å] for $EuAg_4In_8$ at 296(2) K with estimated standard deviations in parentheses.

Label	Distances	Label	Distances
Eu–In1	3.4001 (5)	In1–In1	2.9935 (10)
Eu–In2	3.5458 (5)	In1–In1	3.5699 (3)
Eu–Ag	3.7491 (1)	In1–In2	3.1649 (4)
Ag–Ag	2.8746 (1)	In1–In2	3.1934 (8)
Ag–In1	2.9944 (2)	In1–In2	4.9310 (2)
Ag–In2	2.8635 (1)	In2–In2	2.9359 (9)

2.8. Electrical resistivity

The resistivity measurements were performed in the absence of magnetic field on the single crystals of $EuAg_4In_8$ with a conventional

AC four probe set-up. Four thin copper wires were glued to the pellet using a strongly conducting silver epoxy paste. The data were collected in the range 3–300 K using a commercial Quantum Design Physical Property Measurement System (QD-PPMS). The results were reproducible for up to three batches.

2.9. X-ray absorption near edge spectroscopy (XANES)

X-ray absorption near edge spectroscopy (XANES) experiments at 300 K on $EuAg_4In_8$ were performed at PETRA III, P06 beamline of DESY, Germany. Measurements at the Eu L_{III} edge and at ambient pressure were performed in transmission mode using gas ionization chambers to monitor the incident and transmitted X-ray intensities. Monochromatic X-rays were obtained using a Si (111) double crystal monochromator which was calibrated by defining the inflection point (first derivative maxima) of Cu foil as 8980.5 eV. The beam was focused employing a Kirkpatrick–Baez (K–B) mirror optic. A rhodium coated X-ray mirror was used to suppress higher order harmonics. A CCD detector was used to record the transmitted signals. The sample was prepared by mixing an appropriate amount of finely ground powder with cellulose and cold pressing them to a pellet (Fig. S2).

3. Results and discussion

3.1. Crystal chemistry of $EuAg_4In_8$

The powder XRD of $EuAg_4In_8$ on crushed single crystals is compared with the simulated data obtained from the single crystal structure refinement on the tetragonal and hexagonal systems (shown in Fig. 2). It is well evident that the pattern is perfectly matching with simulated tetragonal crystal system. There are a few additional peaks observed in the hexagonal pattern (marked with ∗), which are absent in the powder XRD of our sample. The absence of a couple of prominent peaks (103) and (203) expected in the hexagonal system (shown in inset of Fig. 2) clearly suggests that our compound was not formed in the reported hexagonal phase. The hexagonal phase reported by Sysa et al. was formed probably due to the difference in the synthesis methods. However, we could not repeat their synthesis method due to the non-technical way of dealing Eu in the arc-melting chamber, which may lead to the Eu deficiency in the resulted product. Another possibility is formation of the hexagonal phase as a metastable phase, which probably resulted due to the rapid quenching of sample from high temperature. Our attempts to synthesize the compound by high frequency induction heating also led to the formation of the mixed phases of tetragonal and hexagonal systems along with unreacted indium and unknown phase (Fig. S1).

The crystal structure of $EuAg_4In_8$ along the *c*-axis is shown in Fig. 3. $EuAg_4In_8$ crystallizes in the $CeMn_4Al_8$ structure type (space group *I*4/*mmm*), which is an ordered superstructure of the $ThMn_{12}$ type. Crystal structure of $EuAg_4In_8$ is composed with pseudo Frank–Kasper cages of 8 Ag atoms and 12 In atoms, which form $[Ag_8In_{12}]$ cages with one europium atom occupied in each ring. These cages are shared through the corner Ag-linkage along the *ab* plane resulting in a three dimensional network. Since the compound was reported in a different structure, it is worth comparing the structures in detail to understand the relations between them. The tetragonal structure consists of only four atomic positions, while hexagonal system is packed with eight atomic coordinates. The crystal structures of tetragonal and hexagonal systems are compared in Fig. 3a (along the *c*-axis) and b (along the *a*-axis), respectively. In order to understand the detailed relations, the structure should be checked layer by layer as drawn in Fig. 3c–g. The tetragonal system is composed of two different types of layers, $[EuIn_4]$ and $[Ag_4In_4]$, while the hexagonal system is composed of three different layers, $[EuIn_6]$, $[Eu_2In_6]$ and $[Ag_{12}In_{12}]$. The layers are arranged in ABABAB and ABCBAB fashion in tetragonal (along the *c*-direction) and hexagonal (along the *a*-direction) systems, respectively. The layer $[EuIn_4]$ in the tetragonal phase and layers $[EuIn_6]$ and $[Eu_2In_6]$ in hexagonal phase are compared in Fig. 3c, d and e respectively. In all these layers, the Ag and In atoms form hexagons and Eu atoms are statistically distributed at the center. The notable difference between the structures is in the arrangement of hexagon rings. In the case of the tetragonal systems, the hexagons are edge shared and propagated along the *c*-direction (Fig. 3c). These layers are well separated with the bond distances of 4.151 Å of In2–In2 atoms and one layer of Eu atoms is sandwiched between them. On the other hand, in the hexagonal system, the hexagons are discrete in one layer C (Fig. 3e) with the bond distance of 3.954 Å of In4–In4 atoms and only dimers in layer A (Fig. 3d). In layer C of the hexagonal system, the Eu atoms are occupied in a triangle trap of three hexagon rings. The appearance of the layers $[Ag_4In_4]$ and $[Ag_{12}In_{12}]$ in the tetragonal and hexagonal systems, respectively shown in Fig. 3f and g are similar with the formation of 4 membered rings of Ag and In atoms. However, a close look at the coordination environments of Ag atoms in the layers suggests that they are substantially different (Fig. 3h and i). In the case of tetragonal system, there is presence of inversion symmetry with equal bond distances of Ag–In1 (2.994 Å) and Ag–In2 (2.863 Å) along with similar In1–Ag–In2 bond angle (65.362 Å). On the other hand, in the case of hexagonal system, the inversion symmetry is lost due to the slight distortion of Ag–In bond (Fig. 3i) angle from 61.792 Å (Ag–Ag–In1) to 64.111 Å (In2–Ag–In3). Overall, the structures are closely related, but as we mentioned earlier, the different synthesis parameters lead to different crystal systems.

In order to check the phase transition from tetragonal to hexagonal, we have done temperature dependent SCXRD studies in the temperature range 100–450 K. Although we have not seen any phase transition in the temperature range 100–450 K, an increment in the lattice parameters and cell volume of the structure was observed (Fig. 4).

The local coordination environments of all atoms in the crystal structure of $EuAg_4In_8$ are presented in Fig. 5. The coordination environment of Eu atom is formed as cages of 20 atoms are composed of 8 Ag and 12 In The coordination environment of Ag atom is made up of a cuboctahedron of $[Eu_2Ag_2In_8]$. Coordination environments of In1 and In2 are composed of $[EuAg_4In_3]$ and $[Eu_2Ag_4In_6]$. The average Ag–Ag bond distance in the $EuAg_4In_8$ crystal structure is 2.8746(1) Å, which is close to the sum of the atomic radii of two Ag atoms (2.871 Å) and is close to the value observed in the previously reported hexagonal $EuAg_4In_8$ structure as well [26]. The average bond distance of Eu–In (3.4729(5) Å) is close to the theoretical distance of 3.44 Å [55]. The bond distance between Eu and Ag atoms is 3.7491(1) Å, which is also close to the radii sum of Eu–Ag atoms (3.75 Å) observed in $EuAg_4In_8$ [26].

3.2. Physical properties

3.2.1. Magnetism

The temperature dependent molar magnetic susceptibility (χ_m) and inverse susceptibility ($1/\chi_m$) of $EuAg_4In_8$ at an applied field of 1000 Oe are shown in Fig. 6. The inverse susceptibility curve obeys Curie–Weiss law, $\chi = C/(T-\theta)$, above 50 K with an effective magnetic moment of 8.26 μ_B/Eu atom, which suggests the existence of divalent nature of Eu atoms. The estimated experimental μ_{eff} value is slightly larger than that expected for a free Eu^{2+} ion moment (7.96 μ_B/Eu), which can be attributed to the conduction electron polarization [56]. However, it is not uncommon that the slight higher values are reported in many rare earth based intermetallic compounds, for example in $EuIrIn_4$ [41], the magnetic moment of Eu ions shows 8.45 μ_B/Eu and Tb_2CuGe_3 the magnetic moment of Tb ions shows 9.72 μ_B/Tb [56]. The divalent nature of Eu was further confirmed by X-ray absorption near edge spectroscopy at Eu L_{III} edge (Fig. S2 of the

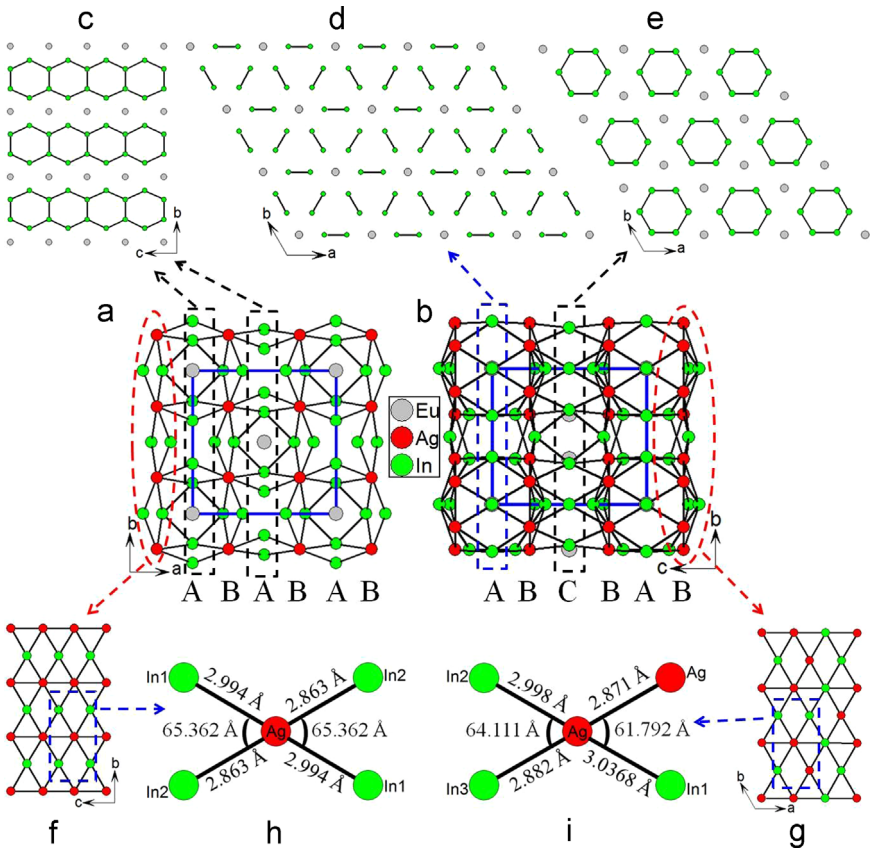

Fig. 3. Crystal structure of $EuAg_4In_8$ (a) tetragonal system along the *c*-axis, (b) hexagonal system along the *a*-axis, unit cell outlined as blue solid lines, (c and f) $EuIn_4$ and Ag_4In_4 two layers are present in tetragonal system, (d, e and g) $EuIn_6$, Eu_2In_6 and $Ag_{12}In_{12}$ three layers are present in hexagonal system and (h and i) coordination environment of Ag atoms in the layers of tetragonal and hexagonal crystal systems.

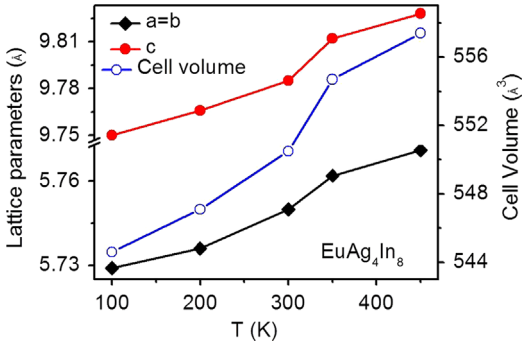

Fig. 4. Temperature dependent single crystal data of $EuAg_4In_8$, lattice parameters and cell volume.

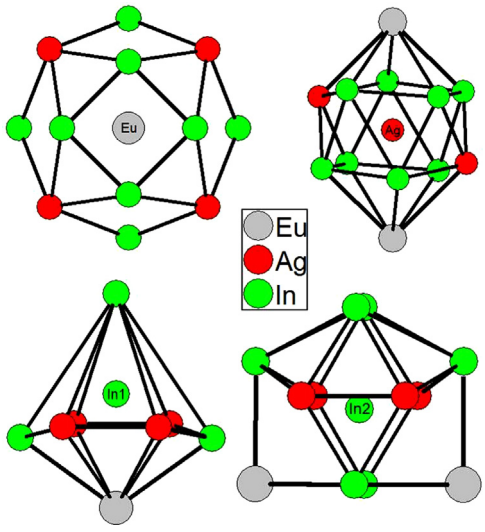

Fig. 5. Coordination sphere of all atoms in the crystal structure of $EuAg_4In_8$ is presented.

Supporting information), which is again in corroboration with the hexagonal phase [26]. Magnetic susceptibility curve of $EuAg_4In_8$ shows an antiferromagnetic ordering around 5.4 K (T_N) (showed in inset Fig. 6).

The field dependence of the magnetization $M(H)$ for ground sample of $EuAg_4In_8$ measured at 2 K and 300 K has been shown in Fig. 7. The data measured at 300 K exhibits linear behavior upto higher magnetic moment obtained at 0.02 emu/mol. The magnetization curve taken at 2 K shows a slight field dependent response up to ~10 kOe and continues to rise slowly up to the highest obtainable field (60 kOe) without any further saturation.

3.2.2. Electrical resistivity

The normal state temperature dependent resistivity (ρ) of $EuAg_4In_8$ continuously decreases linearly with decreasing temperature (shown in Fig. 8), which is typical for metallic systems [57,58]. A weak dip at 4.5 K in the resistivity data shown in inset is in corroboration with the magnetic susceptibility data. The low temperature data (5–10 K) were fitted with power law equation, $\rho=\rho_0+AT^n$ (ρ_0 is the residual resistivity and A and n are the fitting parameters) [59], which yielded a residual resistivity of 1.0 mΩ cm and an n value of 2.11. Thus for this compound at low temperature ρ varies with T^2 which establishes the fact that this compound shows Fermi-liquid behavior at low temperature [31,60,61].

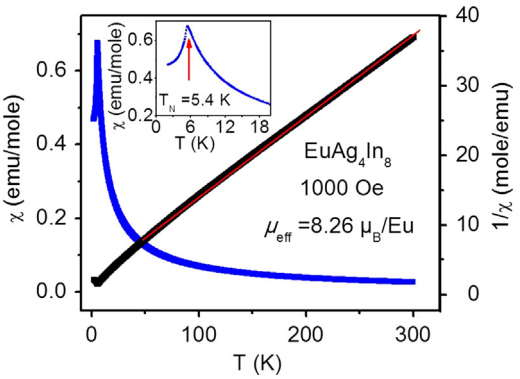

Fig. 6. Temperature dependence of magnetic susceptibility (χ_m) and inverse magnetic susceptibility ($1/\chi_m$) of $EuAg_4In_8$ measured at 1000 Oe.

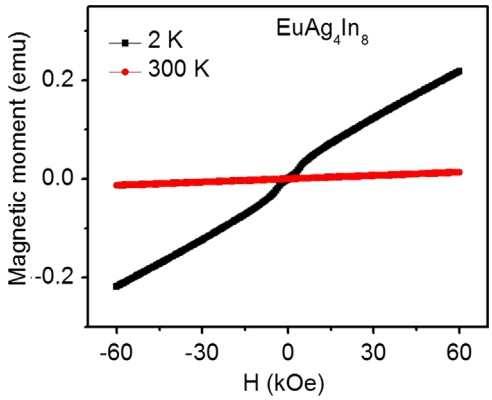

Fig. 7. Magnetization as a function of applied magnetic field at 2 K and 300 K for a single crystal of $EuAg_4In_8$.

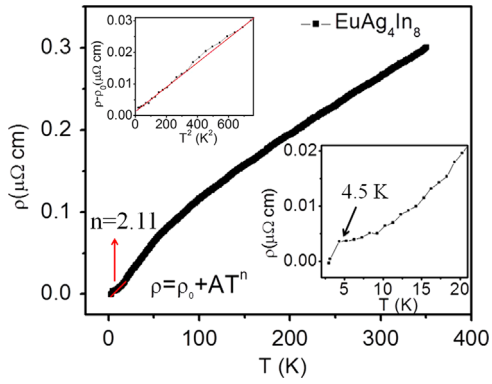

Fig. 8. Temperature dependence of the electrical resistivity (ρ) of $EuAg_4In_8$ with zero applied magnetic field. Inset shows low temperature resistivity data on an expanded scale showing the peaks close to 4.5 K which corresponds to antiferromagnetic ordering.

4. Concluding remarks

The flux method proves to be an excellent tool for growing intermetallic compounds to understand the complex crystal structures. $EuAg_4In_8$ single crystals were obtained from reactions in molten In over a broad range of synthetic conditions. The crystal structure was studied using single crystal X-ray diffraction. The room temperature structure was refined from single crystal diffractometer data revealing tetragonal structure type, which is in contrast to the hexagonal system previously reported. The argument on the existence of the hexagonal phase might have been due to the metastable or superstructure of the well known tetragonal *I*4/*mmm* space group, which in fact may be associated with the different synthesis method. The compound $EuAg_4In_8$ features divalent Eu confirmed by magnetic and XANES measurements. Since Eu is expected to show the valence fluctuation, we also attempted to see any phase transitions within the probable window of temperature range 100–400 K, but resulted in a stable phase. A systematic temperature and magnetic field dependent structural and physical property measurements on $EuAg_4In_8$ might bring out some other interesting physical phenomena.

Supporting information available

Crystallographic information files (CIF), supporting file with powder XRD of the sample synthesized by high frequency induction furnace method and XANES at Eu L_{III} edge. This material is available free of charge via the Internet.

Acknowledgments

We thank Prof. C.N.R. Rao, F.R.S for his support and guidance. We thank Jawaharlal Nehru Centre for Advanced Scientific Research, Department of Science and Technology (DST) and Sheikh Saqr Laboratory (SSL) for the financial support. U.S. and S.S. thank Council of Scientific and Industrial Research (CSIR) for research fellowship and S.C.P. thanks DST, India for Ramanujan fellowship (Grant SR/S2/RJN-24/2010. Thanks to Somnath Ghara for resistivity measurements and Bhavya for SEM measurements. We are thankful to DST and Saha Institute of Nuclear Physics for funding, DESY, Germany for the XANES beamlinend Dr. Gerald Falkenberg for helping the measurements.

Appendix A. Supporting information

Supplementary data associated with this article can be found in the online version at http://dx.doi.org/10.1016/j.jssc.2015.02.013.

References

[1] B. Kindler, D. Finsterbusch, R. Graf, F. Ritter, W. Assmus, B. Luthi, Phys. Rev. B 50 (1994) 704–707.
[2] E. Bauer, Adv. Phys. 40 (1991) 417–534.
[3] P. Wachter, Handbook on the Physics and Chemistry of Rare Earths, Elsevier Science, Amsterdam, 1994.
[4] Y. Matsumoto, S. Nakatsuji, K. Kuga, Y. Karaki, N. Horie, Y. Shimura, T. Sakakibara, A.H. Nevidomskyy, P. Coleman, Science 331 (2011) 316–319.
[5] S. Ernst, S. Kirchner, C. Krellner, C. Geibel, G. Zwicknagl, F. Steglich, S. Wirth, Nature 474 (2011) 362–366.
[6] O. Stockert, J. Arndt, E. Faulhaber, C. Geibel, H.S. Jeevan, S. Kirchner, M. Loewenhaupt, K. Schmalzl, W. Schmidt, Q. Si, F. Steglich, Nat. Phys. 7 (2011) 119–124.
[7] L.S. Hausermannberg, R.N. Shelton, Phys. Rev. B 35 (1987) 6659–6664.
[8] H.F. Braun, C.U. Segre, Solid State Commun. 35 (1980) 735–738.
[9] J.M. Lawrence, P.S. Riseborough, R.D. Park, Rep. Prog. Phys. 44 (1981) 1–84.
[10] Z. Fisk, D.W. Hess, C.J. Pethick, D. Pines, J.L. Smith, J.D. Thompson, J.O. Willis, Science 239 (1988) 33–42.
[11] S. Sarkar, S.C. Peter, J. Chem. Sci. 124 (2012) 1385–1390.
[12] M.G. Kanatzidis, R. Pottgen, W. Jeitschko, Angew. Chem. Int. Ed. 44 (2005) 6996–7023.
[13] C.P. Sebastian, J. Salvador, J.B. Martin, M.G. Kanatzidis, Inorg. Chem. 49 (2010) 10468–10474.
[14] S.C. Peter, S. Sarkar, M.G. Kanatzidis, Inorg. Chem. 51 (2012) 10793–10799.
[15] S.C. Peter, S. Rayaprol, M.C. Francisco, M.G. Kanatzidis, Eur. J. Inorg. Chem. (2011) 3963–3968.
[16] S.C. Peter, C.D. Malliakas, M.G. Kanatzidis, Inorg. Chem. 52 (2013) 4909–4915.
[17] C.P. Sebastian, C.D. Malliakas, M. Chondroudi, I. Schellenberg, S. Rayaprol, R. D. Hoffmann, R. Pottgen, M.G. Kanatzidis, Inorg. Chem. 49 (2010) 9574–9580.
[18] S.C. Peter, M.G. Kanatzidis, Z. Anorg. Allg. Chem. 638 (2012) 287–293.
[19] M. Chondroudi, S.C. Peter, C.D. Malliakas, M. Balasubramanian, Q.A. Li, M. G. Kanatzidis, Inorg. Chem. 50 (2011) 1184–1193.
[20] S.C. Peter, M. Chondroudi, C.D. Malliakas, M. Balasubramanian, M. G. Kanatzidis, J. Am. Chem. Sci. 133 (2011) 13840–13843.
[21] S.C. Peter, M.G. Kanatzidis, J. Solid State Chem. 183 (2010) 2077–2081.
[22] J.G. Mao, J. Goodey, A.M. Guloy, Inorg. Chem. 41 (2002) 931–937.

[23] U. Subbarao, A. Sebastian, S. Rayaprol, C.S. Yadav, A. Svane, G. Vaitheeswaran, S.C. Peter, Cryst. Growth Des. 13 (2013) 352–359.
[24] V.Y. Markiv, N.N. Belyavina, T.I. Zhunkovaskaya, Dopov. Akad. Nauk. Uke. RSR (Ser. A) (1982) 2–80.
[25] U. Subbarao, S.C. Peter, Cryst. Growth Des. 13 (2013) 953–959.
[26] L.V. Sysa, Y.M. Kalychak, I.N. Ctets, Y.V. Galadzhun, Kristallografiya 39 (1994) 821–824.
[27] U. Subbarao, M.J. Gutmann, S.C. Peter, Inorg. Chem. 52 (2013) 2219–2227.
[28] U. Subbarao, S.C. Peter, Inorg. Chem. 51 (2012) 6326–6332.
[29] U. Subbarao, S.C. Peter, J. Chem. Sci. 125 (2013) 1315–1323.
[30] M. Angst, A. Kreyssig, Y. Janssen, J.W. Kim, L. Tan, D. Wermeille, Y. Mozharivskyij, A. Kracher, A.I. Goldman, P.C. Canfield, Phys. Rev. B 72 (2005) 174407–174420.
[31] C.M. Varma, Rev. Mod. Phys. 48 (1976) 219.
[32] M. Godinho, G. Bonfait, A.P. Goncalves, M. Almeida, J.C. Spirlet, J. Magn. Magn. Mater. 140 (1995) 1417–1418.
[33] Y. Verbovytsky, K. Latka, A.W. Pacyna, K. Tomala, J. Alloy. Compd. 438 (2007) L12–L15.
[34] G. Bergerhoff, I.D. Brown, in: F.H. Allen, (Ed.), In Crystallographic Databases, Chester, 1987.
[35] P. Villars, K. Cenzual, Pearson's Crystal Data – Crystal Structure Database for Inorganic Compounds, ASM International, Materials Park, Ohio, USA, 2011.
[36] T.I. Yamson, M.B. Manyako, O.S. Zarechnyuk, Russ. Metall. 6 (1992) 161–165.
[37] I. Felner, I. Nowik, J. Phys. Chem. Solids 40 (1979) 1035–1044.
[38] I. Felner, I. Nowik, J. Phys. Chem. Solids 39 (1978) 951–956.
[39] I. Felner, M. Seh, M. Rakavy, I. Nowik, J. Phys. Chem. Solids 42 (1981) 369–377.
[40] I. Felner, J. Less-Common. Met. 72 (1980) 241–249.
[41] S. Sarkar, M.J. Gutmann, S.C. Peter, Dalton Trans. 43 (2014) 15879–15886.
[42] S. Sarkar, M.J. Gutmann, S.C. Peter, Cryst. Growth Des. 13 (2013) 4285–4294.
[43] S. Sarkar, S.C. Peter, Inorg. Chem. 52 (2013) 9741–9748.
[44] S. Sarkar, M.J. Gutmann, S.C. Peter, CrystEngComm 15 (2013) 8006–8013.
[45] S.C. Peter, U. Subbarao, S. Sarkar, G. Vaitheeswaran, A. Svane, M.G. Kanatzidis, J. Alloy. Compd. 589 (2014) 405–411.
[46] M. Chondroudi, M. Balasubramanian, U. Welp, W.K. Kwok, M.G. Kanatzidis, Chem. Mater. 19 (2007) 4769–4775.
[47] S.C. Peter, U. Subbarao, S. Rayaprol, J.B. Martin, M. Balasubramanian, C. D. Malliakas, M.G. Kanatzidis, Inorg. Chem. 53 (2014) 6615–6623.
[48] U. Subbarao, S. Sarkar, V.K. Gudelli, V. Kanchana, G. Vaitheeswaran, S.C. Peter, Inorg. Chem. 52 (2013) 13631–13638.
[49] U. Subbarao, S.C. Peter, Adv. Mater. Phys. Chem. 3 (2013) 54–59.
[50] SAINT, Bruker AXS Inc., Madison, Wisconsin, USA, 2000.
[51] G.M. Sheldrick, Empirical Absorption Correction Program, SADABS, Göttingen, Germany, 1997.
[52] L.J. WinGX., A windows program for crystal structure analysis: Farrugia, J. Appl. Crystallogr. 32 (1999) 837–838.
[53] G.M. Sheldrick, Acta Crystallogr. A 64 (2008) 112–122.
[54] Diamond, Crystal Impact, Rathausgasse, Bonn, Germany, 2011.
[55] E.V. Sampathkumaran, L.C. Gupta, P.R. Vijayaraghavan, T.K. Hatwar, M. N. Ghatikar, B.D. Padalia, Mater. Res. Bull. 15 (1980) 939–943.
[56] S. Majumdar, E.V. Sampathkumaran, Solid State Commun. 117 (2001) 645–648.
[57] J. He, G. Ling, Z. Jiao, Physica B 301 (2001) 196–202.
[58] R.V. Dremov, N. Koblyuk, Y. Mudryk, L. Romaka, V. Sechovsky, J. Alloy. Compd. 317 (2001) 293–296.
[59] S. Kambe, H. Suderow, T. Fukuhara, J. Flouquet, T. Takimoto, J. Low Temp. Phys. 117 (1999) 101–112.
[60] S.Y. Li, L. Taillefer, D.G. Hawthorn, M.A. Tanatar, J. Paglione, M. Sutherland, R. W. Hill, C.H. Wang, X.H. Chen, Phys. Rev. Lett. 93 (2004).
[61] S.C. Peter, C.D. Malliakas, H. Nakotte, K. Kothapilli, S. Rayaprol, A.J. Schultz, M. G. Kanatzidis, J. Solid State Chem. 187 (2012) 200–207.